Available online at www.sciencedirect.com
ScienceDirect
Journal of Molecular Graphics and Modelling 25 (2006) 77–86
Journal of Molecular Graphics and Modelling
www.elsevier.com/locate/JMGM

# Molecular dynamics characterization of *n*-octyl-β-D-glucopyranoside micelle structure in aqueous solution

Praveen Konidala [a], Lizhong He [b], Bernd Niemeyer [a,c,*]

[a] *Institute of Thermodynamics, Helmut-Schmidt-University/University of the Federal Armed Forces Hamburg, Holstenhofweg 85, D-22043 Hamburg, Germany*
[b] *Center for Nanostructural Bioengineering, University of Queensland, St Lucia QLD 4072, Australia*
[c] *Institute for Coastal Research/Development of Operational Systems, GKSS Research Center, D-21502 Geesthacht, Germany*

Received 2 September 2005; received in revised form 21 November 2005; accepted 21 November 2005
Available online 28 December 2005

**Abstract**

*n*-Octyl-β-D-glucopyranoside (OG) is a non-ionic glycolipid, which is used widely in biotechnical and biochemical applications. All-atom molecular dynamics simulations from two different initial coordinates and velocities in explicit solvent have been performed to characterize the structural behaviour of an OG aggregate at equilibrium conditions. Geometric packing properties determined from the simulations and small angle neutron scattering experiment state that OG micelles are more likely to exist in a non-spherical shape, even at the concentration range near to the critical micelle concentration (0.025 M). Despite few large deviations in the principal moment of inertia ratios, the average micelle shape calculated from both simulations is a prolate ellipsoid. The deviations at these time scales are presumably the temporary shape change of a micelle. However, the size of the micelle and the accessible surface areas were constant during the simulations with the micelle surface being rough and partially elongated. Radial distribution functions computed for the hydroxyl oxygen atoms of an OG show sharper peaks at a minimum van der Waals contact distance than the acetal oxygen, ring oxygen, and anomeric carbon atoms. This result indicates that these atoms are pointed outwards at the hydrophilic/hydrophobic interface, form hydrogen bonds with the water molecules, and thus hydrate the micelle surface effectively.


*Keywords:* Glycolipids; Molecular dynamic simulations; Micelle structure; Radial distribution functions; Aggregate surface

## 1. Introduction

In spite of the combined efforts of experimental and theoretical research performed on surfactant molecules over the last couple of decades [1–4], very few researchers have studied the physico-chemical properties of glycolipids particularly with the molecular dynamics (MD) simulations. Indeed, it is well known that the system orders itself at a certain concentration called critical micelle concentration (cmc) by self-assembling into different aggregate structures according to the type of the lipid molecule. The glycolipids are such non-ionic lipid molecules, consisting of a polar sugar head and a non-polar hydrocarbon chain. The glucosidic bond connects the sugar head group and hydrocarbon tail at the acetal oxygen (O1) atom of the glucose unit (see Fig. 1). The published literature on non-ionic glycolipids states that they are biodegradable, better water soluble, non-toxic, and available from renewable resources compared to the conventional ionic surfactants [5–7].

The primary utilization of *n*-octyl-β-D-glucopyranoside (OG) is in the field of solubilization and crystallization of membrane proteins [8,9]. It is used to preserve the structure of a protein without denaturation. Studies on solubilization of rat lung membrane vasoactive intestinal peptide (VIP) receptors in OG solution indicate that the large amount of OG was bound to the VIP receptor, which is a glycoprotein embedded extensively in the lipid membrane [10]. Being classified as mild detergents, they are imperative in the isolation, purification, and reconstitution of integral membrane proteins from biological membranes to study their intrinsic structural and functional properties [11]. In addition to that, several other important biological applications of the sugar-based lipids are found in ligand–lectin interactions [12] and affinity separation of proteins with ligands [13]. Furthermore, the addition of a small amount of OG (1 wt.%) to the ternary system cetyltrimethylammonium/glycerol/water results in a phase change behaviour, which induces nematic liquid crystals in

* Corresponding author. Tel.: +49 40 6541 3500; fax: +49 40 6541 2008.
*E-mail address:* bernd.niemeyer@hsu-hh.de (B. Niemeyer).

1093-3263/$ – see front matter © 2005 Elsevier Inc. All rights reserved.
doi:10.1016/j.jmgm.2005.11.008

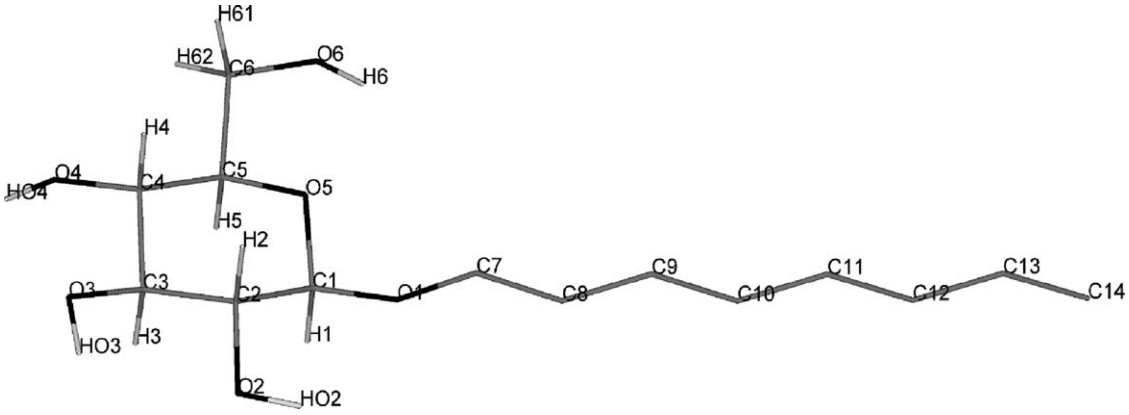


Fig. 1. Structure of an *n*-octyl-β-D-glucopyranoside (OG) molecule with the atom numbering (hydrogen atoms in the hydrocarbon chain were not shown). Sticks represent carbon (grey), oxygen (black) and hydrogen atoms (white).

the solution with the increase of micellar and hexagonal phases [14]. OG has also been employed as drug delivery carriers, food emulsifiers, and in cosmetics and dermatics [15].

The application of atomistic MD simulations to the complex lipids, proteins, and DNA systems in the solution phase is conceivable by a snappy development of computer hardware resources and faster software algorithms. Early MD simulations were very limited and used bead models to describe the system [16–18], and until recently, high end MD simulations with full atomistic models were applied to investigate the properties of the ionic surfactants, such as sodium octanoate [19–24], dodecylphosphocholine [25,26], and sodium dodecyl sulphate [27–29] molecules in the aqueous solution phase. Early reports on OG stated that aggregates of above 10 monomers were more stable and remain intact during the course of the simulation [30]. In addition, the combined study of MD and nuclear magnetic resonance (NMR), observed that 65% of the peptide (protein hairpin turn region) was bound to the OG micelle [31].

Besides that, there are several experimental techniques available to characterize the properties of lipids in the solution. The most frequently used methods for analyzing the micelle structure (aggregation number, molecular geometry, micelle shape, etc.) and dynamic properties were published from small angle neutron scattering (SANS) [32], small angle X-ray scattering (SAXS) [33], NMR [7,31], and Raman and infrared spectroscopy experiments [34]. Most of these methods assume a predefined model to interpret the experimental data. Since the rate of micelle formation and dissociation above cmc is quite fast, it is often very difficult to measure these quantities accurately with the experiments [2,3,7]. Moreover, the purity of sample prepared from the commercial process is expected to have a slight influence on the properties of the OG measured by the experiments [32,35].

In the past, many conflicts in the properties of the OG molecules were reported [30,32]. The expeditious and accurate study of their physical and chemical properties is demanding, and so, we aim to address these issues in this work using the potential OG micelle constructed for this purpose. The results from the MD simulations were analyzed and compared with the SANS experiments performed previously in our lab. The experimental result illustrated that the aggregation number of 90 OG monomers and the micelle structural parameters fitted to the ellipsoidal and cylindrical models were quite reasonable and in accord with other experimental and theoretical works [32]. As a consequence the aggregation number of 92 OG monomers was constructed for the MD simulations, as detailed in the following section.

## 2. Methodology

### 2.1. Initial model building

The solvated glycolipid model used in the simulations was generated by the following two steps. First, a rhombic dodecahedron (RHDO) water cell was created with the lattice parameter $a, b, c = 70$ Å, $(\alpha, \gamma) = 60^\circ$, and $\beta = 90^\circ$ (Fig. 2) [31]. The TIP3P potential model parameters were applied for the water molecules [36]. To remove any existing overlapping

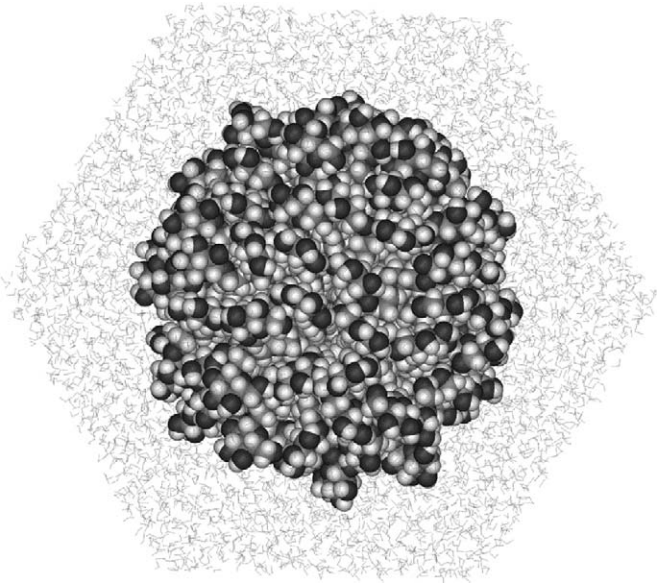

Fig. 2. Rhombic dodecahedron (RHDO) cell prior to the MD simulation. The OG micelle in the center of the cell is represented as van der Waals spheres; oxygen (black), carbon (grey) and hydrogen (white). Water molecules (light gray) surrounding the micelle are made transparent.

atoms between water molecules, the RHDO cell had been minimized with 300 steps of Steepest Descent (SD) and 200 steps of Adopted Basis Newton Raphson (ABNR) method. The resulting coordinates were saved for the heating and equilibration stage followed by a 16 Å hole at the center of the water cell to place the OG micelle at a later stage. Second, a partially spherical micelle was constructed with the software program Insight II from Accelry's Inc. (San Diego, USA). At the beginning, one quarter (23 OG monomers) of the micelle was created by placing the glucose head groups extending outwards and the tails facing inwards to the center. Three copies had been taken out of the first quarter micelle, which had systematically rearranged and joined together without any overlaps to obtain a full spherical micelle of 92 monomers. The partially ordered structure was minimized with 1000 steps of SD and 2000 steps of ABNR to relieve strains or bad contacts that resulted from the manual construction of a micelle. The micelle created in this way was then inserted into the hole of the RHDO water cell, and the water molecules within 2.0 Å of the micelle atoms were deleted, followed by a constrained and unconstrained minimization of the OG micelle. This systematic sequential approach to which we adhered in the present simulations is expected to reduce the equilibration time of the final system to some extent.

### 2.2. Computer experiment details

OG parameters were taken from the CHARMM (Chemistry at Harvard Macromolecular Mechanics) carbohydrate solution forcefield, which is indeed modified from Kuttel et al. [37] forcefield parameters and the references stated therein [38,39] with the fixed partial charges as listed in the Table 1. The MD simulations have been performed with the CHARMM tool [40]. The final solvated system consists of 92 OG monomers and 6796 water molecules, comprising a total of 24,804 atoms present in the RHDO cell (Fig. 2). Periodic boundary conditions (PBC) were imposed to the central cell to mimic the influence of the bulk solvent. The van der Waals non-bonded interactions were terminated at 14 Å with a smooth switching function turned on at a distance of 10 Å and a distance dependent dielectric constant. Non-bonded lists were updated automatically when an atom moved more than 1 Å from the current position. The Particle-Mesh Ewald method was applied for the calculation of electrostatic interactions with 64 grid points for the charged mesh and a sixth order B-spline interpolation [41]. The width of the Gaussian distribution kappa, $\kappa = 0.34$ Å$^{-1}$, was used with the real space cutoff of 14 Å. The bond lengths of all hydrogen atoms were constrained with the SHAKE algorithm [42], and thus, a higher time step of 2 fs has been used for all our simulations. Finally, the whole system was again minimized with the 500 steps of SD and ABNR. The resulting coordinates of the system were employed for the 40 ps of the heating stage in which the system has been heated up from 0 to 298.15 K using the NPT (constant number, pressure, and temperature) ensemble. The reference pressure of 1 atm, pressure piston of 3000 atomic mass units, and a collision frequency of 25 ps$^{-1}$ were maintained in the system [31]. After the system was brought to the desired temperature by coupling to the Hoover thermostat [43], maintained at 298.15 K, several 100 ps, 200 ps, 1 ns, and 2 ns simulations were performed until the 11 ns time scale. The trajectories obtained from these simulations were used for analyzing the structural properties of the OG micelle.

All computations were performed on 64-bit HP Itanium2 SuperDome and SGI Octane2 processors. Benchmark testing from our OG model showed that the HP Itanium2 processor required only one third of the computation time of the Octane2 processor. Because of its excellent performance, we gathered dynamic trajectories for the two large systems of the 11 and 6 ns simulation time scales. The calculations took several weeks with these processors, mainly due to the very large size of the system and the treatment of non-bonded interactions used in the simulations [41].

Table 1
Partial charges of *n*-octyl-β-D-glucopyranoside molecule used in the MD simulations [37–39]

| Atom type (see Fig. 1) | Partial charges |
|---|---|
| O1 | −0.40 |
| C1 | 0.20 |
| O5 | −0.40 |
| C2, C3, C4 | 0.14 |
| C5 | 0.25 |
| O2, O3, O4, O6 | −0.66 |
| HO2, HO3, HO4, H6 | 0.43 |
| C6 | 0.05 |
| C7 | −0.01 |
| C8–C13 | −0.18 |
| C14 | −0.27 |
| All other hydrogens | 0.09 |

## 3. Results and discussion

The average time dependent properties of a micelle in the aqueous solution are computed from the MD simulations carried out with two different initial velocities and coordinates. In general it is assumed that the time average from the MD simulation is the same as the ensemble average obtained by the Monte Carlo simulations or experiments, provided the time average is from a longer run. It will be certainly of great interest either to perform one very long dynamic simulation run for more than few hundred nanoseconds or many simulations with different initial velocities and coordinates to thoroughly characterize all the relevant time dependent properties of the micelles. However, performing such simulations will obviously require enormous computing power. This, in spite of the development in computer hardware resources, is rendered in this work with the two large simulations, one till 11 ns (bog1) and the other till 6 ns (bog2). As seen in Fig. 3, the simulations have converged to a constant average potential energy over the nanosecond time scale. Since both systems have been relaxed, the structural properties investigated are considered to be in a thermodynamic equilibrium state. The bog2 simulation started from different microscopic initial conditions reached steady state immediately after the heating stage (≈40 ps) (black in

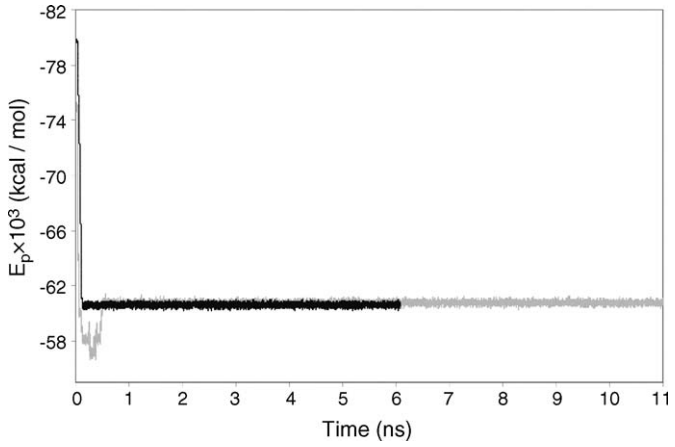


Fig. 3. Potential energy of the bog1 (light gray) and bog2 (black) system with respect to the simulation time.

Fig. 3). Also the structural properties analyzed were more stable than bog1 simulation with little deviations in the micelle shape. Because of these issues we contemplated the bog2 simulation has attained equilibrium faster than bog1 and has been terminated at 6 ns time scale. The completely diffused OG monomers from the central cell are re-centered with respect to the solvent molecules before revealing the dynamic trajectories for cluster analysis. The structure properties from the simulations and experiments are outlined in the following sections.

### 3.1. Structural geometry

The geometry of a monomer has an influence on the structure of the aggregate it forms in the solution in addition to the other factors like ionic strength and temperature. Several geometrical properties (monomer volume, head group area, hydrocarbon chain volume, etc.) were calculated for the OG from the last 1 ns trajectories and averaged (Table 2). The OG head group area in the SANS experiment was taken from Nilsson et al. measured at the hydrophilic/hydrophobic interface [7] and the hydrocarbon tail length of 11.6 Å (maximum length that can be extended) from Tanford [3]. The head group area in MD was calculated from two perpendicular sides of the outermost glucose head group atoms and averaged over the trajectories with the following valid assumptions: (1) the head groups are heavy and difficult to vary in their dimension, (2) the solution temperature is constant, and (3) there were no ions present in the solution that could influence the area of the head group [7,44]. The critical packing factor of 0.59 (bog1), 0.57 (bog2), and 0.52 calculated from MD simulations and SANS suggest that the OG micelle is not spherical. In spite of some small differences in the geometric properties listed in Table 2, good agreement has been obtained for the critical packing parameter between simulations and experiment.

Table 2
Structural geometric properties of an OG calculated from MD simulations, SANS experiment [32] and the literatures stated therein measured at 25 °C

| | MD simulations | | SANS/ literature data |
|---|---|---|---|
| | bog1 | bog2 | |
| Monomer volume (Å$^3$) | 404.5 | 403.7 | 422.0[a] |
| Head group volume (Å$^3$) | 194.5 | 194.3 | 179.4 |
| Head group area, $a_h$ (Å$^2$) | 42.9 | 43.5 | 40[b] |
| Hydrocarbon chain volume, $v_c$ | 210.0 | 209.4 | 242.6[c] |
| Hydrocarbon chain length, $l_c$ (Å) | 8.2 | 8.3 | 11.6[d] |
| Monomer length (Å) | 14.6 | 14.8 | 14.8 |
| Packing factor | 0.59 | 0.57 | 0.52 |

[a] Monomer volume calculated from the apparent molar volume [32].
[b] Head group area/OG at the air-aqueous solution interface [7,37].
[c] Calculated from Tanford [3] at 25 °C.
[d] Maximum possible hydrocarbon chain length that can be extended at 25 °C [3].

MD investigations on micelle aggregates demonstrated in the present work and elsewhere [20,22,30] demonstrates that the hydrocarbon chains were not fully extended inside the micelle core. The existence of trans-gauche dihedral angles causes the hydrocarbon chains to decrease from the extended state. The glucose head group areas and the hydrocarbon tail length calculated from the simulations were reasonable, and the resulting packing factor indicates that the decrease in head group area or hydrocarbon chain length will increase the packing factor value. The dimensionless packing factor obtained from the SANS experiment performed at cmc and the MD simulations at 0.62 M concentration agree well with each other and prove that the spherical micelles are impossible to form with their molecular geometry (Table 2), even at the very low concentration region measured by the SANS [32,45]. According to Israelachvili [46], the packing factor of ∼0.50 leads to cylindrical micelles in the solution. The author calculated a packing factor of 0.37 for the sodium dodecyl sulfate and 0.85 for the phosphatidylcholine aggregates with the energetically favoured spherical shape for the first and flexible bilayer or vesicle shape for the latter. In summary, because of its bulky rigid head group and small single hydrocarbon (octyl) chain, the packing factor of above 0.50 for the OG micelle calculated from both MD simulations is more favorable to a cylindrical shape in accordance with the SANS experiments [32,45].

### 3.2. Aggregate shape

Characterization of the micelle dynamic shape and surface is important particularly when the aggregates in the solution are highly anisotropic, deviating significantly from the spherical/symmetric shape. Moment of inertia tensors were calculated from the coordinates of the system and the corresponding eigenvalues are diagonalized to obtain three principal moments of inertia. Analyzing the ratios of the three principal moments of inertia ($I_1/I_3$, $I_2/I_3$, and $I_1/I_2$) provides accurate shape transformations of the aggregate in the solution (Fig. 4) [24,26,47]. It is interesting to see from these ratios that large fluctuations in the OG system have occurred at a couple of infrequent intervals over the 11 ns time scale. Nevertheless, the three average moment of inertia ratios calculated from the entire dynamic trajectories were 1.4, 1.3, 1.1 (bog1) and 1.3,

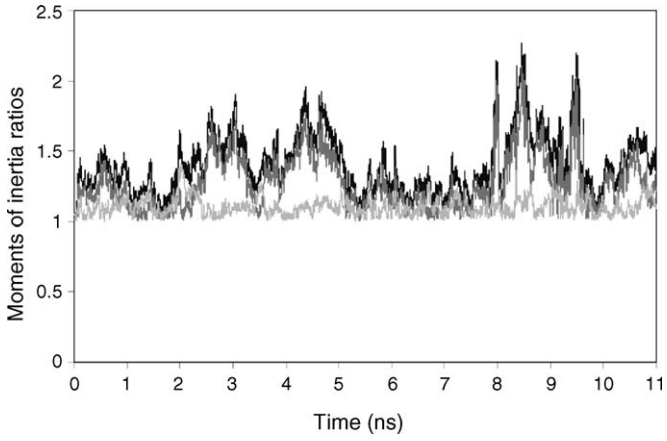


Fig. 4. Principal moment of inertia ratios of the OG micelle from bog1 simulation. $I_1/I_3$-ratio of largest to the smallest principal axis (black), $I_2/I_3$-ratio of intermediate to the smallest principal axis (dark gray), $I_1/I_2$-ratio of largest to the intermediate principal axis (light grey).

1.2, 1.1 (bog2). The far lowest principal moment of inertia ratio ($I_1/I_2$) of 1.1 (light gray in Fig. 4) compared to the other two ratios in the bog1 simulation indicates that the micelle is a prolate ellipsoid (semi axes $a = b$). The micelle in the bog2 simulation was more compact with the ratios a little closer to each other (i.e. the monomers in the micelle stay closer and remain intact). One or rarely two monomers are diffused out of the micelle during the course of the dynamic run in the bog2 simulation in contrast to the bog1 simulation (see Fig. 5).

Similarly, Tieleman et al. [26] calculated the moment of inertia ratios of 1.4, 1.3, and 1.0 from the dodecylphosphocholine (DPC) simulations performed on the aggregate size of 40 monomers. They also observed from their longer simulation that a major shape change of a micelle occurred for the 54 DPC monomers, leading to less spherical shape on the time scale of above 8 ns (see Fig. 3 from ref. [26]). The same behaviour was observed in our bog1 simulations at around 3, 4.5, and 8–9.5 ns (see Fig. 4). At these time scales, the two moment of inertia ratios deviate significantly from the third lower ratio. The OG micelle was most often in a prolate ellipsoidal form but sometimes also have a small bilayer-like or rod shaped cylindrical form. The deviations seem to be that the OG micelle tries to restructure its shape into a more complex shape at these instants, but the governing thermodynamic conditions, in particular, the concentration region we simulated, the geometric constraints of a monomer, and the fixed glucose head group areas at the hydrophobic/hydrophilic interface did not facilitate the formation of such a large asymmetric structure [7], and so, it starts fluctuating at these time scales. We conclude from these results that major shape fluctuations in the micelle are always there in the isotropic concentration region, which keeps the OG micelle a small sized ellipsoid or cylindrical rod [45].

In addition, visual inspection of trajectories from the bog1 simulation at the 9 ns time scale gave further clues to the overall micelle diffusion and rotation in the solution [48]. A small part of the micelle has been diffused out of the RHDO cell at one corner and the completely escaped monomers reentered into the cell in the opposite direction (see Fig. 5c). In spite of the micelle monomers re-centered in the central cell for the analysis of moment of inertia ratios, larger fluctuations in the system were observed. Because of these translational and rotational motions of the micelle, we suspect that at some point of time, the whole micelle may diffuse out of the RHDO cell (much longer MD simulation needed than the current run) and reenter from the opposite side of the cell.

The eccentricity ($e$) of an OG micelle was calculated from the principal moment of inertia ratios to observe the elongation of the micelle. The $e$ value of 0.62 calculated in this work is consistent with $e = 0.60$ from the Bogusz et al. [30] simulations performed on the same molecule. As is evident, the micelle was elongated, but it did not extend to a bilayer or needlelike rod ($e = 1.0$), at least in the present simulations of 92 OG monomers. The aggregate size studied here is much higher than the simulations reported by the aforementioned authors. We observed temporary large shape fluctuations encountered in the solution at a nanoseconds range with the increase in concentration (0.62 M). La Mesa et al. [49] have showed a similar trend through their dielectric and viscosity experiments that the micelle shape has a slight and continuous influence on the surfactant concentration. Increasing the aggregate size to well above 100 OG monomers might result in the formation of bilayer or complex asymmetric structures in the solution with increasing eccentricities, which is a subject beyond the scope of this work.

### 3.3. Accessible surface area (ASA)

The surface change of a micelle from the ordered spherical shape (Fig. 5a and d) to the partial asymmetric structure (Fig. 5c and f) over time is reflected by the increase in ASA at the beginning of the simulations for the glucose heads and hydrocarbon tails as shown in Fig. 6. The method developed by Lee and Richards [50] was used with a probe radius of 1.4 Å (to mimic water) rolled over the surface of the micelle to calculate the ASA. The ASA of the OG head was constant over the 11 ns simulation (bog1), but the ASA of hydrocarbon tail shows some deviations at the 9.5 ns time scale. As already seen from the preceding section, there were major changes in the micelle shape that occurred at these time scales (Fig. 4). The fluctuations in the micelle shape increased the hydrophobic patches. As a consequence, a higher fraction of hydrocarbon chains are exposed to the hydrophilic environment (dark gray in Fig. 6). These results ensure that very large fluctuations (moment of inertia ratios of above 2.0) in the shape will affect the hydrophobic surface area of the micelle, whereas the smaller fluctuations would not affect the local structure of the monomers significantly [26].

After few hundred picoseconds, the ASA for the OG head, tail, and the total monomer remained at an average value of 12,800, 3300, and 16,100 Å$^2$ for the bog1 simulation and 12,700, 3100, and 15,800 Å$^2$ for the bog2 simulation, respectively. The major contribution of the glucose head (139.5 Å$^2$/glucose head (bog1)) and (138.4 Å$^2$/glucose head (bog2)) to the total monomer ASA (175.2 Å$^2$/OG monomer (bog1)) and (172.0 Å$^2$/OG

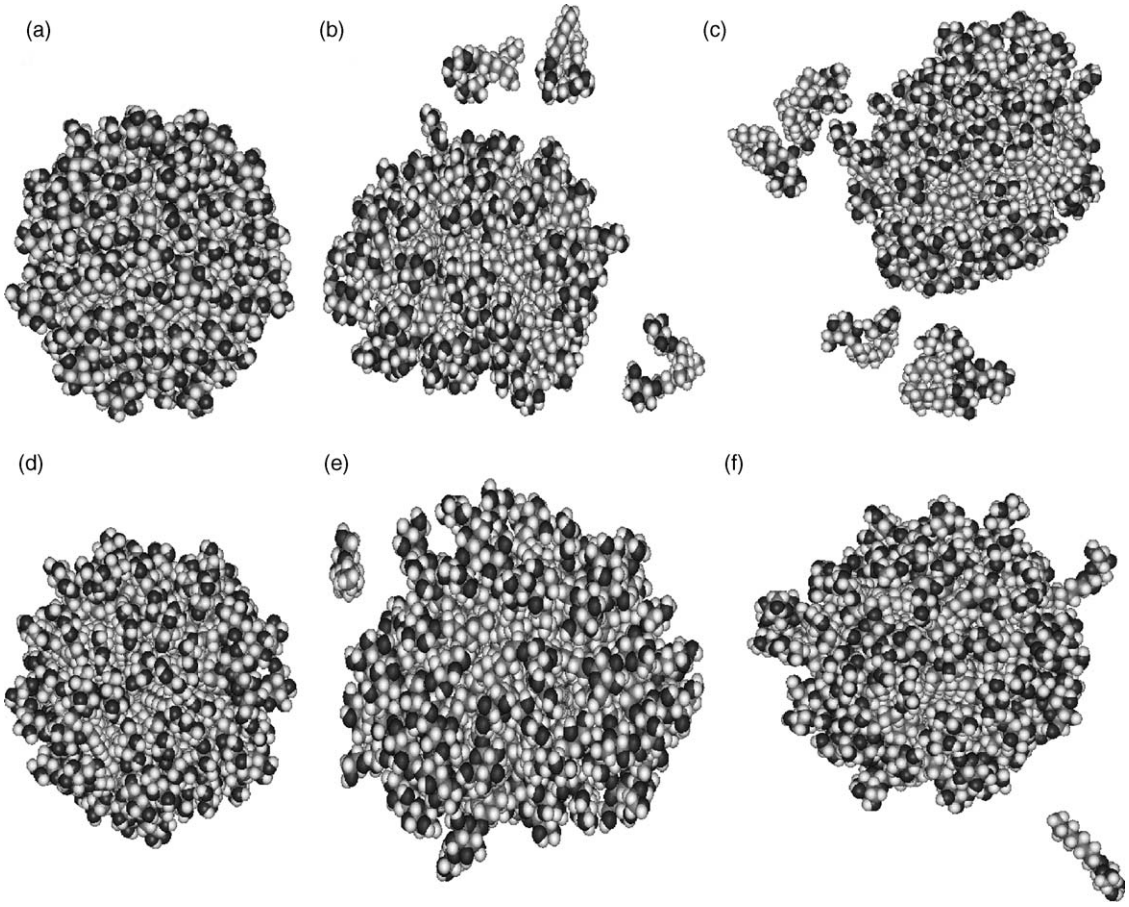


Fig. 5. Snapshot of the OG micelle from bog1 simulation at time (a) $t = 0$ ns, (b) $t = 6$ ns, (c) $t = 11$ ns and bog2 simulation at time (d) $t = 0$ ns, (e) $t = 3$ ns (f) $t = 6$ ns time scales. Water molecules are blanked for clarity. Colors are as of Fig. 2.

monomer (bog2)) is due to the surface roughness and micelle elongation [27]. The rough surface causes water molecules to stay on the micelle surface and interact with the glucose head group atoms. As expected, the contribution of the hydrocarbon tail (35.7 Å$^2$/tail (bog1)) and (33.6 Å$^2$/tail (bog2)) (Fig. 6) to the total ASA is low because large portions of the chains are facing towards the micellar core thereby avoiding contact with water.

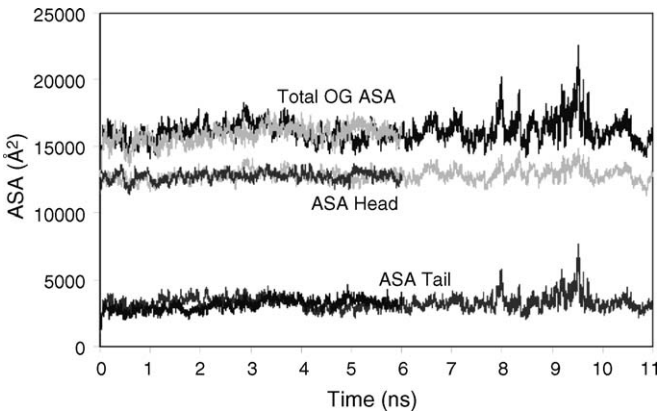


Fig. 6. Total accessible surface areas of an OG micelle (black), glucose heads (light grey) and hydrocarbon tails (dark grey) from the bog1 simulation (11.0 ns). Also shown in the same plot the ASA's of bog2 simulation till 6.0 ns time scale with different color contrast.

The tail ASA in the bog2 simulation is lower than in the bog1 because the structure of the micelle is more compact and prevents hydrocarbon chains from coming into contact with the water molecules.

The ratio of tail/total ASA obtained for our 92 OG monomers is 20%, which is higher than the ratio of 12% reported for the 67 OG monomers [31]. Dixon et al. presumed that increasing the size of the OG micelle would reduce the hydrophobic patches exposed to the solvent molecules. Our results confirm that increasing the OG aggregate size (around 90 monomers) will certainly increase the exposure of hydrocarbon tails to the water molecules as long as the micelles are asymmetric in structure. Because of its non-spherical shape and partially elongated micelle structure, a higher fraction of hydrocarbon chains were exposed to the water molecules [27].

### 3.4. Radius of gyration ($R_g$)

The radius of gyration, a measure of the aggregate size, was calculated from the trajectories stored during the dynamic run. It was also observed to check the equilibration of the system in addition to the usual potential energy fluctuations [23,24]. OG monomers those were fully diffused from the RHDO box had been re-centered for the gyration radius cluster analysis. An

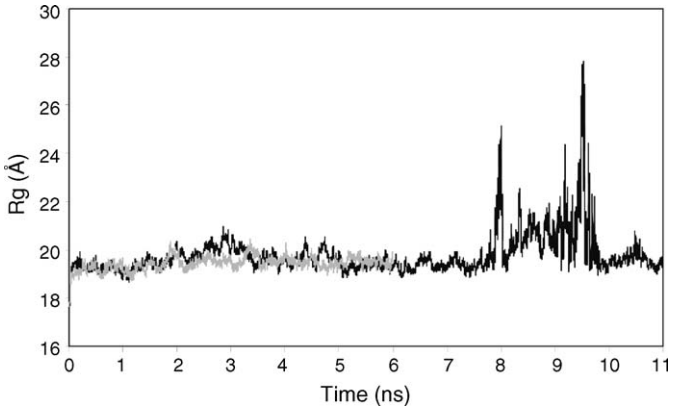


Fig. 7. OG micelle radius of gyration calculated from the bog1 (black) and bog2 (light grey) simulations as a function of time.

average $R_g$ value of 19.8 Å (bog1) (black in Fig. 7) and 19.4 Å (bog2) (light grey in Fig. 7) was calculated for the OG micelle from both trajectories. The size of the micelle was constant over the simulation time scales except at around 9 ns where larger fluctuations in the system were observed (Fig. 7). At these time scales, the OG micelle is more disordered, and the monomers are broadly distributed into the solution, thus increasing the size of the micelle instantaneously.

In summary, the radius of gyration calculated from the 11 ns (bog1) trajectories showed that the micelle size in the solution did not increase with time. Because of its polar nature and the fixed geometric areas of the head groups [7], it exerts a strong hydration force from the aqueous solution [33,49], which prevents the formation of large anisotropic micelle. The micelle grows very quickly near to the cmc. Once it covers the surface with enough glucose head groups consistent with the molecular geometry and free energy requirements of the system, an increase in the number of monomers will not increase the size of the micelle in the isotropic solution region [45]. Instead, it starts releasing monomers back into the solution, similar to the snapshot of the trajectory shown in Fig. 5. This proves that the micelle tries to be small and short ranged; no ordering of the micelle to bilayer has taken place in the concentration region simulated in this present work.

The SANS experimental $R_g$ values of the OG micelle differed significantly from the MD results. An $R_g$ value of 29.4 and 29.1 Å have been calculated using ellipsoidal and cylindrical models from the SANS experiments measured at 0.1 M concentration [32]. On the other hand, Nilsson et al. [7] calculated an $R_g$ value of 40 Å from SAXS experiment and 17 Å from the two-shell model with spherical micelle core of 11.7 Å and a shell thickness of 5 Å. These variations are often observed between experiments themselves and with the theory due to different experimental operating conditions, sample purity, and the treatment of the several parameters of the potential dynamic model. Previous MD simulations reported an average $R_g$ of 17.6 Å for the aggregate size of 75 OG monomers [30]. Their results show a linear increase of $R_g$ for the different aggregate sizes they studied, which is consistent with our simulations. In addition, the size of our micelle shows very good agreement with the D'Aprano et al. [45] SANS experiments. They calculated an $R_g$ of 19 Å for a size of the cylinder at the concentration close to the cmc.

### 3.5. Micelle–water interactions

The interaction of solvent molecules with the monomer reference atoms is deduced by the radial distribution functions (RDF) constructed between different atoms of the OG monomer and oxygen atom of the water molecules [47]. The hydroxyl oxygen atoms of the glucose head group and oxygen atom of the water molecules show sharp peaks at a distance of 2.8 Å in the RDF's shown in Fig. 8. This is the minimum van der Waals diameter between any two oxygen atoms separated by a distance called contact distant $d$ [51]. The second peak appears at a distance of approximately 5.6 Å and reflects the sum of the diameters of the oxygen atoms. It is clear that these atoms are interacting directly with the aqueous environment without any obstructions from the remaining micelle atoms. The presence of micelle atoms at the interface of the aqueous region causes a disruption of the water–hydrogen bonding network [29]. The disturbed water molecules then form hydrogen bonds to the head group atoms and interact with the micelle surface.

The magnitude of the peaks for the ring oxygen (O5) atom (grey line in Fig. 9) and the acetal oxygen (O1) atom (black line in Fig. 9) shows an approximately one third reduction of water molecules in the first hydration shell compared to the hydroxyl oxygen atoms. A broader peak area is obtained for these atoms in the second hydration shell due to the ordering of the water molecules near the surface of the micelle. The steric hindrance caused by the other micelle atoms lowers the contact of water in the first hydration shell where most of these oxygen atoms are facing inwards (away from the bulk water) in the direction of the micellar hydrocarbon core. A similar trend has also been observed for the anomeric carbon (C1) atom (black line in Fig. 10) and the C7 carbon atom in the hydrocarbon chain connected to the glucose head (black dotted line in Fig. 10). In

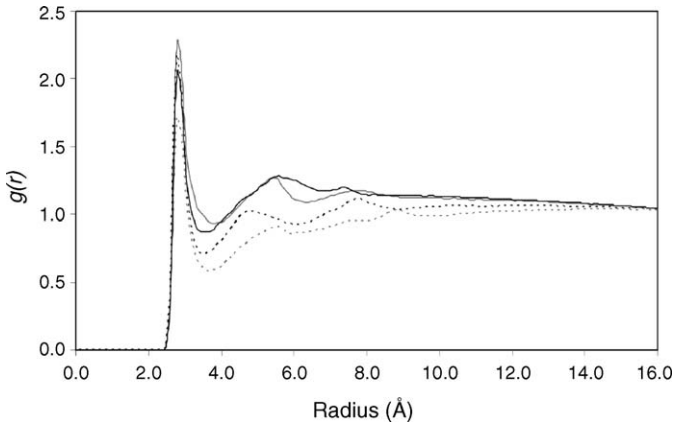


Fig. 8. Radial distribution functions of hydroxyl oxygen atoms in the glucose head with the water oxygen ($O_w$) atoms. Refer to Fig. 1 for the atom numbering. O2–$O_w$ (grey dotted), O3–$O_w$ (grey), O4–$O_w$ (black), O6–$O_w$ (black dottted).

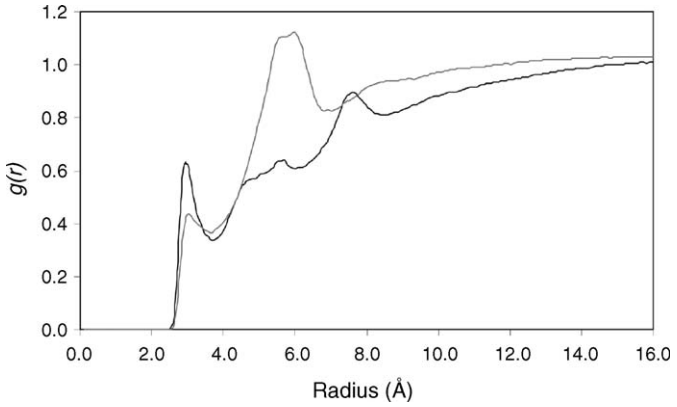


Fig. 9. Radial distribution functions of ring oxygen (O5) and acetal oxygen (O1) atoms with the water oxygen ($O_w$) atoms. Refer to Fig. 1 for the atom numbering. O1–$O_w$ (black), O5–$O_w$ (grey).

Table 3
Average hydration number per OG calculated for the glucose oxygen atoms, anomeric carbon atom (C1), and C7 carbon atom within a radius of 3.0 and 5.0 Å

| Atom number (refer Fig. 1) | Hydration number/OG ($r$ = 3.0 Å) | | Hydration number/OG ($r$ = 5.0 Å) | |
|---|---|---|---|---|
| | bog1 | bog2 | bog1 | bog2 |
| O2 | 0.96 | 0.98 | 5.28 | 5.37 |
| O3 | 1.30 | 1.32 | 7.90 | 8.16 |
| O4 | 1.18 | 1.22 | 7.95 | 8.26 |
| O6 | 1.20 | 1.22 | 6.64 | 6.72 |
| O1 | 0.31 | 0.31 | 3.20 | 3.21 |
| O5 | 0.18 | 0.18 | 3.47 | 3.44 |
| C1 | [a] | [a] | 3.60 | 3.64 |
| C7 | [a] | [a] | 2.73 | 2.76 |

[a] Average number of water molecules for these atoms are negligible ($r \leq 3.0$ Å $\approx 0$).

addition, the RDF for the whole hydrocarbon chain and water is shown in the Fig. 10 (grey line) where all the peaks are diffused meaning that there was no considerable number of water molecules involved in the interaction with the hydrocarbon chains. Of course, there may be few water molecules near the acetal oxygen atoms in some OG monomers, which lead to small peaks, but they are negligible compared to the head group atoms.

Analyzing the RDF plots of oxygen atoms of OG, we conclude that all hydroxyl atoms in the OG head are primarily involved in the hydration of the micelle. The appearance of sharp pronounced peaks at 2.8 Å (Fig. 8) for these atom types in the RDF plots are due to β conformation of the OG monomer [7] (Fig. 1) and the surface roughness of the micelle [27]. In general, the micelle elongation and the presence of an anisotropic rough surface allow water molecules to penetrate into the gaps and interact with the head group atoms efficiently, as compared to the other amphiphilic molecules [22,27]. As seen in Fig. 8 ($g(r) \approx 2$ at $r = 2.8$ Å), the number of water molecules near the OG hydroxyl oxygen atoms is about two times higher than the number in bulk water. The water molecules are organized onto the micelle surface and interact with the OG head with a disruption in the hydrogen-bonding network [29].

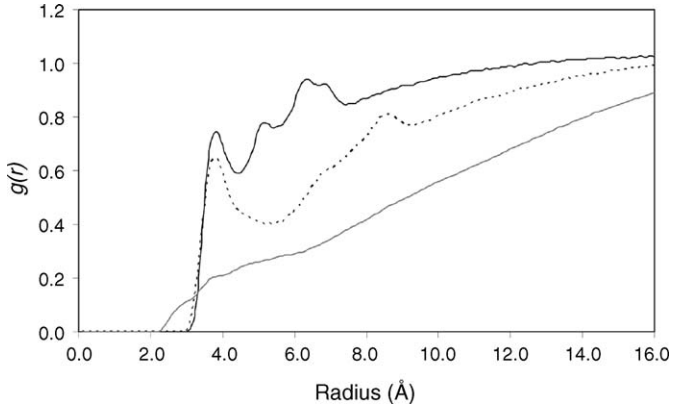


Fig. 10. Radial distribution functions of anomeric carbon (C1) atom, C7 carbon atom in the hydrocarbon chain connected to the glucose head and the whole hydrocarbon chain with the water oxygen ($O_w$) atoms. Refer to Fig. 1 for the atom numbering. C1–$O_w$ (black), C7–$O_w$ (black dotted), octyl chain–$O_w$ (grey).

The reduction of water molecules for the O1 and O5 atoms is evident from the average hydration number calculated within a radius of 3.0 and 5.0 Å (Table 3). Integration of the areas within a 5.0 Å distance in the RDFs ensures that the O1 and O5 atoms are 2.1 times lower in average hydration number than the hydroxyl oxygen atoms (see Table 3) from both simulations. Verifying the data within the radius of 3.0 Å for the O1 and O5 atoms for both simulations shows that the average hydration number of 0.25 is 13 times lower in average hydration number 3.3 for the same atoms within 5.0 Å distance, whereas the difference is only around 6 times for the hydroxyl oxygen atoms between these distances. Published experimental values for the average hydration number per glucose head group are between 4–12 water molecules [7,32,49]. We determined that the average hydration number per glucose head group within 5.0 Å of the OG head from both simulations is around 7 water molecules, which is consistent with the experimental values.

## 4. Conclusions

Molecular dynamics simulation results presented in this paper characterize the structural properties of an OG micelle in aqueous solution. Depending on the individual conformation of a molecule, several issues come into play when it starts aggregating into different structures above cmc. The critical packing parameter implies that due to the geometric constraints of the glucose head group area and hydrocarbon chain length, the micelle formed is not likely to have a spherical shape, even at the concentrations close to the cmc [32]. A packing factor of above 0.50 was calculated from the simulations and experiment.

Accurate shape transformations of the micelle in the solution were studied from the principal moment of inertia ratios from which it was discovered that the OG micelle was most often in a prolate ellipsoidal form with two similar and one smaller moment of inertia ratios [26,30]. An interesting behaviour has

also been observed from the 11 ns simulation. The micelle seems to be in a small bilayer or cylindrical rod form at some infrequent intervals where large deviations in the two principal moment of inertia ratios occurred, as compared to the third lowest ratio [26]. In order to characterize such dynamic events (i.e. micelle shape fluctuations which arise at arbitrary time scales due to underlying thermodynamic forces, geometric constraints, and different initial coordinates and velocities) completely, the MD simulations have to be carried out for very long time scales and with many different initial coordinates [48], which could be computationally taxing.

Two simulations that started with different initial velocities and coordinates showed that micelle size and ASA remained constant except at one instant (around 9 ns) in the bog1 simulation where large deviations in the principal moment of inertia ratios of above 2.0 were observed. In summary, the OG micelle is small and short ranged; no ordering of the micelle to bilayer took place in the concentration region studied in this work [7]. The $R_g$ calculated from the simulations was consistent with some experimental and theoretical results [30,45]. The contribution of ASA of the glucose head to the total ASA of the monomer is relatively high compared to that of the hydrocarbon tail due to the surface roughness and elongation of micelle. Radial distribution functions constructed for different atoms of the monomer confirm that hydroxyl oxygen atoms at the hydrophilic/hydrophobic interface are more strongly hydrated than the acetal oxygen, ring oxygen, and anomeric carbon atoms, which face outward towards the aqueous environment. This indispensable knowledge that emerged from analyzing the structural properties of an OG micelle at atomistic scale simulations will be very helpful in the field of biotechnical applications and glycoconjugate research and processing [9–11,13].

## Acknowledgment

We thank Dr. Rick Venable, FDA/CBER/OVRR Biophysics Lab, Maryland, for the delightful discussions and support.

## References

[1] A. Patist, J.R. Kanicky, P.K. Shukla, D.O. Shah, Importance of micellar kinetics in relation to technological processes, J. Colloid. Interface Sci. 245 (2002) 1–15.
[2] I. Danielsson, Thermodynamic aspects of micelle formation, Finska Kemists. Medd. 72 (1963) 90–98.
[3] C. Tanford, The Hydrophobic Effect: Formation of Micelles and Biological Membranes, second ed., John Wiley & Sons, New York, 1980.
[4] K. Shinoda, T. Yamanaka, K. Kinoshita, Surface chemical properties in aqueous solutions of non-ionic surfactants: octyl glycol ether, α-octyl glyceryl ether and octyl glucoside, J. Phys. Chem. 63 (1959) 648–650.
[5] A.J.J. Straathof, H. van Bekkum, A.P.G. Kieboom, Solid state and solution properties of octyl D-glucopyranosides, Starch/Stärke 40 (1988) 438–440.
[6] A.J.J. Straathof, H. van Bekkum, A.P.G. Kieboom, efficient preparation of octyl α-D-glucopyranoside monohydrate: A recirculation procedure involving water removal by product crystallization, Starch/Stärke 40 (1988) 229–234.
[7] F. Nilsson, O. Soederman, I. Johansson, Physical-chemical properties of the *n*-octyl β-D-glucoside/water system. A phase diagram, self-diffusion NMR, and SAXS study, Langmuir 12 (1996) 902–908.
[8] R.J. Gould, B.H. Ginsberg, A.A. Spector, Effect of octyl β-glucoside on insulin binding to solubilized membrane receptors, Biochemistry 20 (1981) 6776–6781.
[9] R.M. Garavito, J.P. Rosenbusch, Isolation and crystallization of bacterial porin, Methods Enzymol. 125 (1986) 309–328.
[10] S. Patthi, M. Akong, G. Velicelebi, Hydrodynamic characterization of vasoactive intestinal peptide receptors extracted from rat lung membranes in triton X-100 and *n*-octyl-β-D-glucopyranoside, J. Biol. Chem. 262 (1987) 15740–15745.
[11] M. le Maire, P. Champeil, J.V. Moller, Interaction of membrane proteins and lipids with solubilizing detergents, Biochim. Biophys. Acta 1508 (2000) 86–111.
[12] L.-Z. He, S. Andre, H.-C. Siebert, H. Helmholz, B. Niemeyer, H.-J. Gabius, Detection of ligand- and solvent-induced shape alterations of cell-growth-regulatory human lectin galectin-1 in solution by small angle neutron and X-ray scattering, Biophys. J. 85 (2003) 511–524.
[13] W.C. Lee, K.H. Lee, Applications of affinity chromatography in proteomics, Anal. Biochem. 324 (2004) 1–10.
[14] A.B. Cortes, M. Valiente, The effect of a minimum amount of octyl-β-D-glucoside on micellar, nematic, and hexagonal phases of the CTAB/glycerol/water system, Colloid. Polym. Sci. 281 (2003) 319–324.
[15] H. Kiwada, H. Nimura, Y. Fujisaki, S. Yamada, Y. Kato, Application of synthetic alkyl glycoside vesicles as drug carriers. I. Preparation and physical properties, Chem. Pharm. Bull. 33 (1985) 753–759.
[16] B. Smit, P.A.J. Hilbers, K. Esselink, L.A.M. Rupert, N.M. van Os, A.G. Schlijper, Computer simulations of a water/oil interface in the presence of micelles, Nature 348 (1990) 624–625.
[17] S. Karaborni, N.M. van Os, K. Esselink, P.A.J. Hilbers, Molecular dynamics simulations of oil solubilization in surfactant solutions, Langmuir 9 (1993) 1175–1178.
[18] K. Esselink, P.A.J. Hilbers, N.M. van Os, B. Smit, S. Karaborni, Molecular dynamics simulations of model oil/water/surfactant systems, Colloid. Surf. A 91 (1994) 155–167.
[19] K. Watanabe, M. Ferrario, M.L. Klein, Molecular dynamics study of sodium octanoate micelle in aqueous solution, J. Phys. Chem. 92 (1988) 819–821.
[20] H. Kuhn, H. Rehage, The molecular structure of sodium octanoate micelles studied by molecular dynamics computer experiments, Ber. Bunsenges. Phys. Chem. 101 (1997) 1485–1492.
[21] H. Kuhn, B. Breitzke, H. Rehage, The phenomenon of water penetration into sodium octanoate micelles studied by molecular dynamics computer simulation, Colloid. Polym. Sci. 276 (1998) 824–832.
[22] L. Laaksonen, J.B. Rosenholm, Molecular dynamics simulations of the water/octanoate interface in the presence of micelles, Chem. Phys. Lett. 216 (1993) 429–434.
[23] A.F. Moura, L.C.G. Freitas, Molecular dynamics simulation of the sodium octanoate micelle in aqueous solution: Comparison of force field parameters and molecular topology effects on the micellar structure, Braz. J. Phys. 34 (2004) 64–72.
[24] H. Kuhn, B. Breitzke, H. Rehage, A molecular modelling study of pentanol solubilized in a sodium octanoate micelle, J. Colloid. Interface Sci. 249 (2002) 152–161.
[25] S.J. Marrink, D.P. Tieleman, A.E. Mark, Molecular dynamics simulation of the kinetics of spontaneous micelle formation, J. Phys. Chem. B 104 (2000) 12165–12173.
[26] D.P. Tieleman, D. van der Spoel, H.J.C. Berendsen, Molecular dynamics simulations of dodecylphosphocholine micelles at three different aggregate sizes: Micellar structure and chain relaxation, J. Phys. Chem. B 104 (2000) 6380–6388.
[27] C.D. Bruce, M.L. Berkowitz, L. Perera, M.D.E. Forbes, Molecular dynamics simulation of sodium dodecyl sulfate micelle in water: Micellar structural characteristics and counterion distribution, J. Phys. Chem. B 106 (2002) 3788–3793.
[28] S. Bandyopadhyay, M.L. Klein, G.J. Martyna, M. Tarek, Molecular dynamics studies of the hexagonal mesophase of sodium dodecylsulphate in aqueous solution, Mol. Phys. 95 (1998) 377–384.
[29] C.D. Bruce, S. Senapati, M.L. Berkowitz, L. Perera, M.D.E. Forbes, Molecular dynamics simulations of sodium dodecyl sulfate micelle in water: The behavior of water, J. Phys. Chem. B 106 (2002) 10902–10907.

[30] S. Bogusz, R.M. Venable, R.W. Pastor, Molecular dynamics simulations of octyl glucoside micelles: Structural properties, J. Phys. Chem. B 104 (2000) 5462–5470.
[31] A.M. Dixon, R.M. Venable, R.W. Pastor, T.E. Bull, Micelle-bound conformation of a hairpin-forming peptide: Combined NMR and molecular dynamics study, Biopolymers 65 (2002) 284–298.
[32] L.-Z. He, V. Garamus, B. Niemeyer, H. Helmholz, R. Willumeit, Determination of micelle structure of octyl-β-glucoside in aqueous solution by small angle neutron scattering and geometric analysis, J. Mol. Liq. 89 (2000) 239–249.
[33] L.-Z. He, V. Garamus, S.S. Funari, M. Malfois, R. Willumeit, B. Niemeyer, Comparison of small-angle scattering methods for the structural analysis of octyl-β-maltopyranoside micelles, J. Phys. Chem. B 106 (2002) 7596–7604.
[34] I. Laczko-Hollosi, M. Hollosi, V.M. Lee, H.H. Mantsch, Conformational change of a synthetic amyloid analogue des[Ala21,30]A42 upon binding to octyl glucoside micelles, Eur. Biophys. J. 21 (1992) 345–348.
[35] B. Lorber, J.B. Bishop, L.J. DeLucas, Purification of octyl beta-D-glucopyranoside and re-estimation of its micellar size, Biochim. Biophys. Acta 1023 (1990) 254–265.
[36] S.R. Durell, B.R. Brooks, A. Ben-Naim, Solvent-induced forces between two hydrophilic groups, J. Phys. Chem. 98 (1994) 2198–2202.
[37] M. Kuttel, J.W. Brady, K.J. Naidoo, Carbohydrate solution simulations: Producing a force field with experimentally consistent primary alcohol rotational frequencies and populations, J. Comput. Chem. 23 (2002) 1236–1243.
[38] R. Palma, M.E. Himmel, G. Liang, J.W. Brady, Molecular mechanics studies of cellulases, in: M.E. Himmel (Ed.), Glycosyl Hydrolases in Biomass Conversion, American Chemical Society, Washington DC, 2001.
[39] S.N. Ha, A. Giammona, M. Field, J.W. Brady, A revised potential-energy surface for molecular mechanics studies of carbohydrates, Carbohydr. Res. 180 (1988) 207–221.
[40] B.R. Brooks, R.E. Bruccoleri, B.D. Olafson, D.J. States, S. Swaminathan, M. Karplus, CHARMM: A program for macromolecular energy, minimization, and dynamics calculations, J. Comput. Chem. 4 (1983) 187–217.
[41] U. Essmann, L. Perera, M.L. Berkowitz, T. Darden, H. Lee, L.G.J. Pedersen, A smooth particle mesh ewald method, J. Chem. Phys. 103 (1995) 8577–8593.
[42] J.P. Ryckaert, G. Ciccotti, H.J.C. Berendsen, Numerical integration of the cartesian equation of motion of a system with constraints: molecular dynamics of *N*-alkanes, J. Comput. Phys. 23 (1977) 327–341.
[43] W.G. Hoover, Canonical dynamics: Equilibrium phase-space distributions, Phys. Rev. A 31 (1985) 1695–1697.
[44] P.S. Goyal, V.K. Aswal, Micellar structure and inter-micelle interactions in micellar solutions: Results of small angle neutron scattering studies, Curr. Sci. 80 (2001) 972–979.
[45] A. D'Aprano, R. Giordano, M.P. Jannelli, S. Magazu, G. Maisano, B. Sesta, QELS and SANS studies of octyl-β-glucoside micellar solutions, J. Mol. Struct. 383 (1996) 177–182.
[46] J.N. Israelachvili, Intermolecular and Surface Forces, second ed., Academic Press, London, 1998.
[47] X. Gao, T.C. Wong, Molecular dynamics simulation of adrenocorticotropin (1–10) peptide in a solvated dodecylphosphocholine micelle, Biopolymers 58 (2001) 643–659.
[48] S. Bogusz, R.M. Venable, R.W. Pastor, Molecular dynamics simulations of octyl glucoside micelles: Dynamic properties, J. Phys. Chem. B 105 (2001) 8312–8321.
[49] C. La Mesa, A. Bonincontro, B. Sesta, Solution properties of octyl β-D-glucoside. Part 1: Aggregate size, shape and hydration, Colloid. Polym. Sci. 271 (1993) 1165–1171.
[50] B. Lee, F.M. Richards, The interpretation of protein structures: Estimation of static accessibility, J. Mol. Biol. 55 (1971) 379–400.
[51] E. Matteoli, G.A. Mansoori, A simple expression for radial distribution functions of pure fluids and mixtures, J. Chem. Phys. 103 (1995) 4672–4677.